



## Observation of electron conics by Juno: implications for radio generation and acceleration processes.

P. Louarn<sup>1</sup>, F. Allegrini<sup>2,3</sup>, D. J. McComas<sup>7,2</sup>, P. W. Valek<sup>2,3</sup>, W. S. Kurth<sup>5</sup>, N. André<sup>1</sup>, F. Bagenal<sup>4</sup>, S. Bolton<sup>2</sup>, R. W. Ebert<sup>2</sup>, M. Imai<sup>5</sup>, S. Levin<sup>6</sup>, J. R. Szalay<sup>7</sup>, R. J. Wilson<sup>4</sup>

1. Institut de Recherche en Astrophysique et Planétologie (IRAP), Toulouse, France
2. Southwest Research Institute, San Antonio, Texas, USA
3. University of Texas at San Antonio, San Antonio, Texas, USA
4. Laboratory for Atmospheric and Space Physics, University of Colorado, Boulder, Colorado, USA
5. University of Iowa, Iowa City, Iowa, USA
6. Jet Propulsion Laboratory, Pasadena, California, USA
7. Princeton University, Princeton, New Jersey, USA

### Key Points:

- Electron conics are observed by Juno in Jovian radio sources and their role in the wave amplification is analyzed.
- The observed conics may very efficiently drive the cyclotron maser, from decametric to kilometric wavelength ranges.
- The formation of conics is modeled by a stochastic acceleration due to a low frequency parallel electric field turbulence.

This article has been accepted for publication and undergone full peer review but has not been through the copyediting, typesetting, pagination and proofreading process which may lead to differences between this version and the Version of Record. Please cite this article as doi: 10.1029/2018GL078973

**Index Terms:** 2756, 6220, 2483, 7847

### **Abstract**

Using Juno plasma, electric and magnetic field observations (from JADE, Waves and MAG instruments), we show that electron conic distributions are commonly observed in Jovian radio sources. The conics are characterized by maximum fluxes at oblique pitch angles,  $\sim 20^\circ$ - $30^\circ$  from the B-field, both in the upward and downward directions. They constitute an efficient source of free energy for the cyclotron maser instability. Growth rates of  $\sim 3\text{-}7 \times 10^4 \text{ s}^{-1}$  are obtained for hectometric waves, leading to amplification by  $e^{10}$  with propagation paths of 50-100 km. We show that stochastic acceleration due to interactions with a low frequency electric field turbulence located a few  $10^4$  km above the ionosphere may form the observed conics. A possible source of turbulence could be inertial Alfvén waves, suggesting a connection between the auroral acceleration and generation of coherent radio emissions.

### **Plain Language Summary**

Jupiter, as many astrophysical magnetized objects, is a powerful emitter of non-thermal radio emissions. The coherent process required for their generation is likely the Cyclotron Maser Instability (CMI). However, the exact conditions of wave amplification are not known precisely at Jupiter. With Juno mission, for the first time, it is possible to explore the auroral regions of Jupiter, where the particles are accelerated and the non-thermal emissions produced. With several crossing of the radio sources, the free energy used by the CMI can now be identified. It corresponds to 'conic-like' distributions, characterized by an accumulation of particles just outside the loss-cones. Applying the CMI theory, large growth rates are obtained, showing that the conics probably play a central role in the wave generation

source. The formation of the conics could be due to an interaction with a low frequency Alfvénic turbulence. This suggests a close relationship between the radio wave generation and the particle acceleration, as at Earth, the details of the scenario being, nevertheless, slightly different.

## 1 Introduction

Since its arrival in July 2016, Juno regularly crosses the polar regions of Jupiter and acquires high quality plasma and wave measurements in its auroral regions [Bagenal *et al.*, 2017]. This offers an exceptional opportunity to investigate the *in-situ* properties of intense jovian radio emissions and understand the coherent process required for their generation. In particular, the observations from JADE [McComas *et al.*, 2013], Waves [Kurth *et al.*, 2017a], and MAG [Connerney *et al.*, 2017] instruments provide measurements at the required precision to determine the features of the electron distribution that may drive the cyclotron maser instability (CMI), the most likely generation process. This is essential to establish the scenario of the radio wave amplification.

The CMI theory has been the subject of many studies and is well supported by observations (see Wu [1985] and Zarka [1998] for reviews). This kinetic instability amplifies X mode waves at frequencies close to the electron gyrofrequency in a tenuous plasma ( $\epsilon = (f_p/f_c)^2 \ll 1$  where  $f_p$  and  $f_c$  are respectively the electron plasma and gyrofrequency) provided that the electron distribution ( $f$ ) contains free energy associated with positive  $\partial f / \partial v_{\perp}$  gradients ( $v_{\perp}$  is the velocity perpendicular to the ambient B-field). In the initial version of the CMI [Wu and Lee, 1979], the free energy is linked to a loss cone.

At Earth, it is established that the Auroral Kilometric Radiation (AKR) is generated in localized plasma depleted regions, where the electron distributions present ‘trapped’ or ‘horse-shoe’ populations [Louarn *et al.*, 1990, Delory *et al.*, 1998]. These are also the regions

of parallel acceleration located above the aurora. Electrons at keV energies are dominant, which decreases the gyrofrequency by the relativistic effect. Positive  $\partial f / \partial v_{\perp}$  gradients at  $\sim 90^{\circ}$  pitch angle can then be used by the CMI, leading to a particularly efficient amplification [Pritchett, 1986, Le Quéau and Louarn, 1989, Louarn et al., 1990]. This scenario significantly differs from the ‘loss cone’ CMI.

● Interestingly, the first Juno observations appeared to support the ‘loss cone’ scenario. Louarn et al. [2017] (see also [Kurth et al., 2017b]) have shown that the positive  $\partial f / \partial v_{\perp}$  gradients observed in a source of hectometric radiation (HOM) are associated with the loss cone. Typical CMI growth rates of  $10^4 \text{ s}^{-1}$  are obtained from the measured distribution, leading to amplification paths of  $\sim 1000 \text{ km}$  which is less than the size of the sources crossed by Juno. The characteristics of the amplified waves are consistent with Waves observations [Kurth et al., 2017b, Louis et al., 2017]. The possible role of the loss cone CMI at Jupiter was already studied by Hess et al., [2007] and Mottez et al., [2010] to explain radio-telescope observations of the so-called ‘S-bursts’. The first Juno’s in-situ measurements thus show that the CMI scenario may apply to more general radio emissions.

← With more source crossings, the scenario can be refined. In particular, we show here that ‘conic-like’ features are often superimposed to the loss cones seen in the sources. The distributions are then characterized by maxima of the phase space density at pitch angles just outside of the loss cone limit. Electron conics were first described by Menietti and Burch [1985] using DE-1 observations. They were commonly observed with Viking, in association with low-frequency parallel electric fields [Andre and Eliasson, 1992; Eliasson et al., 1996], suggesting that they are related to auroral acceleration. However, since they do not characterize the dominant free energy in AKR sources, they were seldom considered as a driver of the CMI. In contrast, we show that those observed at Jupiter lead to large CMI growth rates and may be dominant in the generation process.

We first focus on a few examples of conics measured in radio sources (section 2). The CMI growth rates are estimated in section 3, and a model of the formation of the conics is discussed in section 4 before discussion and conclusions in section 5.

## 2 Observations of electron conics in a source of hectometric radiation.

● Wave and electron measurements obtained inside a hectometric radiation (HOM) source are displayed in Figure 1. They have been performed during perijove 5, at 2.5 jovian radii ( $R_J$ ), 3:40 LT and L-shell of  $\sim 14.7$  (VIP4 model with no current sheet). Panel (a) shows the dynamic spectra observed from 7:20 to 7:50, at 0.5-3 MHz. The increase of intensity from  $\sim 7:30$  to 7:38, at  $f_c$  (1.3 MHz), is typical of the crossing of a radio source. The spectral flux locally reaches  $\sim 4 \times 10^{-10} \text{ V}^2 \text{ m}^2 \text{ Hz}^{-1}$  at  $f_c$ , which is an order of magnitude larger than in adjacent regions or at other frequencies.

In panel (b), the increase followed by a decrease of the electron energy, from 7:33:40 to 7:34:15, is consistent with an inverted-V structure, a characteristic feature of auroral electron acceleration (*Hultqvist et al*, 1988). The peak energy increases up to  $\sim 10$  keV. The pitch angle plot (panel c) shows that the distributions are strongly anisotropic, with phase space densities  $\sim 10$  times larger in cones of  $\sim 35^\circ$  aperture in the parallel and anti-parallel directions than at other angles. More detailed plots (panels d and e) reveal the existence of a double loss cone, from  $0^\circ$  to  $\sim 15^\circ$  (upward direction) and  $\sim 165^\circ$  to  $180^\circ$  (downward). The flux then peaks at  $\sim 25-30^\circ$  and  $150-155^\circ$  which defines conic-like distributions. These conics are observed during  $\sim 35$  s ( $\sim 500-1000$  km in Jupiter frame) when the radio flux is maximum at  $f_c$ . This coincides with the inverted-V and suggests that the conics characterize the accelerated electrons populating the radio source. The absence of downward beams (at  $180^\circ$ ) implies that the acceleration occurs below Juno. Consequently, the upward conic would be generated by

an acceleration process occurring close to the ionosphere, with a similar process in the conjugate hemisphere to explain the downward conic.

Another source crossing is shown in figure 2, observed during perijove 4, at  $\sim 1.6 R_J$ ,  $\sim 18:50$  MLT and L-shell of 12. The maximum flux is observed from 13:35 to 13:38, at frequencies close to 6 MHz, with a source crossing around 13:37:30. Two pitch angle distributions measured in the source are displayed. The conics are obvious, with a double loss cone and maximum fluxes at  $20\text{-}30^\circ$  and  $150\text{-}160^\circ$ , just outside of the loss-cones.

We note that the phase space density fluctuates from one energy sampling to the next. This common observation is due to a combined effect of the JADE-E sampling method and flux variations at sub-second scales. To provide the highest cadence within available resources, the high voltage of JADE-E electrostatic analyzer indeed follows a sawtooth profile with measurements made at every second step of the sweep, at a few  $10^{-3}$  s intervals. Thus, if one energy is sampled during the ascent profile, the next is during the descent, a few 0.1 s later. Non-natural fluctuations at adjacent energies are then expected in case of rapid flux variations. The observations thus suggest the existence of significant flux variations at sub-second time scales.

As seen in Figures 1 and 2, the conics exhibit the positive  $\partial f / \partial v_\perp$  gradients needed to drive the CMI. They are seen in parallel/anti-parallel directions, meaning that upward and downward propagating waves may be amplified. This important difference with the classical loss cone may increase the CMI efficiency.

In Table S 1, 13 radio source crossings, identified during perijoves 1 to 7, are listed. Conics are observed in 9 radio sources, often both in the upward and downward directions and superimposed to the loss cones. They may be measured for few consecutive seconds or several times, separately. This first analysis shows that the conics are present in radio sources

in a majority of cases (more than 60% occurrence), from decametric to kilometric radiation.

As shown now, they are efficient drivers of the CMI.

### 3 Estimate of the cyclotron maser growth rate.

The CMI theory is detailed in *Wu and Lee* [1979], *Wu* [1985], *Le Quéau et al.*, [1984 a, b], *Pritchett* [1986]. The simplified version used by *Louarn et al.*, [2017] is adapted to the amplification of X mode waves propagating at frequencies close to  $f_c$ , for  $kc/\omega \sim 1$  ( $k$  is the wave vector), in a low density ( $\epsilon = (\omega_p/\omega_c)^2 \ll 1$ ) and moderately energetic ( $E \ll m_e c^2$ ) plasma. The growth rate is given by:

$$\frac{\gamma}{\omega_c} \sim 2\pi^2 \Delta\omega^2 \int_0^\pi d\theta b^2 \sin(\theta)^2 \frac{\partial}{\partial \beta_\perp} f(\beta_0 + b \cos(\theta), b \sin(\theta)), \quad (1)$$

where:  $\beta_{\perp,\parallel} = (v_{\perp,\parallel}/c)$ ,  $\beta_0 = k_\parallel c/\omega_c$ ,  $\Delta\omega = (\omega - \omega_c)/\omega_c$  and  $b = (\beta_0^2 - 2\Delta\omega)^{1/2}$ .  $f$  is the normalized electron distribution ( $\int f dv^3 = 1$ ). This formula expresses that the growth rate is obtained by integrating  $\partial f/\partial \beta_\perp$  along a resonant circle defined by  $(\beta_\parallel - \beta_0)^2 + \beta_\perp^2 - (\beta_0^2 - 2\Delta\omega) = 0$  (circle with center  $\beta_0$  and radius  $b$ ). The most amplified waves should have circles of resonance lying in the phase space region of positive  $\partial f/\partial v_\perp$ , thus for conics, cones with aperture of  $\sim 25$ - $30^\circ$ , aligned or anti-aligned with the magnetic field, at 1-5 keV.

The growth rate is estimated with a distribution measured in the source described in Figure 1. In pitch angle (figure 3, panel a), one again notes the fluctuations of the phase space density which is likely an indication of fast flux variations. In the following, we consider the  $\partial f/\partial \beta_\perp$  gradients calculated with average and maximum fluxes. They are shown in panel (b). The gradients calculated from  $0^\circ$  to  $25^\circ$  and  $155^\circ$  to  $180^\circ$  are shown in black. They are positive and drive the maser. Those calculated from  $25^\circ$  to  $45^\circ$  and  $135^\circ$  to  $155^\circ$ , in blue, are negative and contribute to the wave absorption. The extremal envelopes (continuous lines) correspond to the maximum phase space density and the dashed lines to the average values. Positive  $\partial f/\partial \beta_\perp$  larger than  $2000 \text{ s}^3 \text{ km}^{-6}$  are measured for  $|v_\parallel|$  varying from  $1.5$  to  $3.5 \cdot 10^7$

m/s ( $\sim 0.5$  to  $\sim 3.5$  keV) in the extremal case. They are 2-3 times smaller for the average distribution.

The growth rates  $\gamma/\omega$  are shown in panel (c) and (d), for resonant circles with center  $\beta_0$  varying from 0.06-0.18 and radius  $b$  from 0.01-0.08. This corresponds to waves propagating at  $87^\circ$  to  $80^\circ$  from the B-field, at frequencies 0.16% to 1.6 % above  $f_c$ . A density of  $10 \text{ cm}^{-3}$  is used, in agreement with JADE measurements.  $\gamma/\omega_c$  as large as 0.007 are obtained in the extremal case and 0.004 in the average case. At  $\sim 1.5$  MHz, this leads to maximum growth of  $7 \times 10^4 \text{ s}^{-1}$  (extremal case) and  $4 \times 10^4 \text{ s}^{-1}$  (average case). This is a strong instability: at light speed, propagations of  $\sim 40$  km (extremal case) or  $\sim 80$  km (average case) are sufficient to amplify the waves by a factor  $e^{10}$ .

As discussed in *Louarn et al* [2017], the efficiency of the instability can also be estimated from its frequency bandwidth. It is  $\sim 0.5$  % here, as deduced from the range of  $b$  corresponding to positive growth. The bandwidth determines the altitude over which a given wave may be amplified before the instability is quenched due to the spatial variation of the gyrofrequency. Over an altitude range  $\Delta h$ , the gyrofrequency varies as  $\Delta f_c/f_c \sim 3 \Delta h/R$ , where  $R$  is the distance from Jupiter center ( $R \sim 2.5 R_J$ ). A bandwidth of 0.5 % then corresponds to  $\Delta h \sim 100$  km and, thus, to a path of 500-1000 km for propagation angles of  $80^\circ$ - $85^\circ$ . Using the estimated growth rates, this leads to amplification larger than  $e^{40}$ . These enormous values mean that the amplification is most likely non-linearly saturated, by quasi-linear relaxation or wave/particle trapping processes [*Le Quéau et al.*, 1984 a, b, *Pritchett*, 1986].

To conclusion, the observed conics can very efficiently drive the CMI, with growth rates about a factor 5-10 larger than with the classical loss cone.

#### **4 Formation of electron conics**

Different mechanisms may generate electron conics. Generally, they include perpendicular or parallel heating due to wave-interactions and mirror effects to transfer the heating to

oblique angles [Eliasson *et al.*, 1996, Menietti and Weimer, 1998; Thompson and Lysak, 1996]. With Juno, we observe conics that are above the acceleration region since precipitating field-aligned beams are not measured simultaneously. These conics were studied by Eliasson *et al.* [1996]. They suggested that an acceleration by a low frequency parallel electric field is a likely formation mechanism. We investigate a similar process except that we consider an interaction with a low frequency turbulence rather than a monochromatic electric field. Turbulence located at one end of a close field line may form mono-directional conics, at both ends double conics.

The low frequency fluctuations can be associated with Alfvén wave turbulence as is commonly observed in Earth. This turbulence leads to the formation of finite parallel electric fields able to accelerate particles provided that the perpendicular wavelengths become close to the electron skin depth [Goertz and Boswell, 1979, Louarn *et al.*, 1994, Kletzing, 1994, Génot *et al.*, 2001, Chaston *et al.*, 2002]. To model the turbulent interaction, we introduce  $P(\Delta W)$ , the probability that the particle energy varies by  $\Delta W$ . Noting  $f_0(W)$  the initial energy distribution of particles, the fraction of particles of initial energy  $W$  reaching an energy  $W_1$  after the interaction is  $f_0(W)P(W_1-W)$ . The final distribution,  $f_1(W_1)$ , is given by the summation of all possibilities:

$$f_1(W_1) = \int_0^{+\infty} f_0(W) P(W_1 - W) dW \quad (2)$$

For the precipitating electrons,  $P(\Delta W)$  can be a shifted Gaussian probability:

$$P(\Delta W) = \frac{1}{\sqrt{2\pi}} \frac{1}{D} \exp \left[ -\frac{1}{2} \frac{(\Delta W - W_0)^2}{D^2} \right] \quad (3)$$

$W_0$  is the average energy gain and  $D$  an energy dispersion. Both are related to the typical potential drop associated with the kinetic Alfvén waves. Values from a few keV to a few tens of keV are reasonable. Combining formula (2) and (3), one describes the net energy gain of

the precipitating electrons and a thermal spread. Conversely, electrons that are reflected due to the mirror effect do not gain energy on average so that  $P(\Delta W)$  becomes a simple Gaussian:

$$P(\Delta W) = \frac{1}{\sqrt{2\pi}} \frac{1}{D} \exp\left[-\frac{1}{2} \frac{\Delta W^2}{D^2}\right] \quad (4)$$

Since we consider  $E_{\parallel}$  turbulence, the probability law affects the distribution of parallel velocities only. Starting with an initial maxwellian distribution:

$$f_0(v_{\parallel}, v_{\perp}) = \left(\frac{m}{2\pi kT}\right)^{\frac{3}{2}} \exp\left[-\frac{1}{2} m \frac{v_{\parallel}^2 + v_{\perp}^2}{kT}\right], \quad (5)$$

with simple algebra, formula (2) and (4) lead to:

$$f_1(v_{\parallel}, v_{\perp}) = \frac{1}{\sqrt{2\pi}} \frac{1}{D} f_0(v_{\parallel}, v_{\perp}) \int_{-\infty}^{\frac{1}{2}mv_{\parallel}^2} \exp\left[\frac{\Delta W}{kT} - \frac{1}{2} \frac{\Delta W^2}{D^2}\right] d\Delta W. \quad (6)$$

If  $D$  is constant, this describes parallel heating, the degree of heating increasing with  $D$ . However, the model can be adapted to match the conics. In particular, we implement a loss cone and consider an inhomogeneous turbulence –i.e. a level of turbulence that increases approaching ionosphere. A more efficiently heating of the electrons that mirror just above the ionosphere –with pitch angles just outside of the loss cone – is then expected. This is precisely the characteristic of the conics.

The effect of the stratified turbulence can be described using a Gaussian probability (formula 4), assuming that the parameter  $D$  varies with the distance to the ionosphere. We consider the following model:

$$D(z) = \alpha + \beta \exp\left[-\frac{(z - L_0)^2}{\delta^2}\right] \quad (7)$$

$z$  is the distance from Juno and  $L_0$  is the distance to the ionosphere.  $\alpha$  and  $\beta$  have the dimension of energy (keV). This model expresses that the fluctuations peak close to the

ionosphere, with some spatial spread, determined by  $\delta$ . For simplicity, we use a linear model of the magnetic field:  $B(z) = B(1 + z/H)$  with  $H=R/3$ . The mirror altitude is then given by:  $z_M = H \left( v_{\parallel} / v_{\perp} \right)^2$ , where  $(v_{\parallel}, v_{\perp})$  are the particle velocity at  $z=0$  (the Juno position). The effect of the stochastic acceleration is then investigated using  $D(z_M)$  in formula (5) and (6). We further assume that the field lines are closed with Alfvén wave turbulence at both ends so that the electrons may interact with the turbulence near their two mirror points to form the double conics.

A simulation example is given in figure 4. We choose an initial Maxwellian with a temperature of 0.5 keV. The ionosphere is placed at  $L_0=25 H$  to get a realistic loss cone. The effects of turbulence are parametrized by  $\alpha=1$  kV,  $\beta=10$  kV and  $\delta=7 H$ , corresponding to turbulence that extends up to 0.4-0.5  $R_J$  above the ionosphere, which is reasonable based on our knowledge of Earth's auroral regions.

It is assumed that the turbulence develops at both ends of the field line. Starting with an initial Maxwellian, the downward conic is obtained from a first interaction in the conjugate hemisphere. This downward conic is then used as a starting distribution for the interaction taking place below Juno. This leads to the upward conic. The successive interactions progressively empty the flux tube. This is counterbalanced by a 5 % regeneration using the initial Maxwellian at each interaction.

As seen in figure 4, the model reproduces the main features of the observed conics. The electrons are heated at pitch angles just outside the loss-cones; their temperature reaches 4-5 keV in a sector of pitch angles extending from the loss cone ( $\sim 15^\circ$ ) to  $\sim 30-35^\circ$ , both in the upward and downward directions. The perpendicular temperature remains close to the initial temperature (0.5 keV, in the present case).

The model is based on 5 free parameters:  $T$  the initial temperature,  $\alpha$ ,  $\beta$  and  $\delta$  that determine the stratified turbulence and the regeneration coefficient ( $\rho$ ). Variations by a factor

2 of  $\alpha$ ,  $\beta$ ,  $\delta$ ,  $\rho$  do not noticeably affect the characteristics of the conics. This suggests that their formation does not require very specific conditions: an absorbing ionosphere and a form of stochastic acceleration in the 10 keV range at both ends of closed field lines would be sufficient. This could be linked to inertial Alfvén turbulence, which is known to be common in Earth's auroral regions.

## 5 Discussion and conclusion

In conclusion, Juno observations reveal that electron conic distributions are common in the jovian radio sources. They are characterized by large phase space densities, at pitch angles just outside the loss cone, at  $\sim 20^\circ$ - $30^\circ$  from the B-field. They are an efficient source of free energy for the CMI, leading to amplification by  $e^{10}$  with propagation paths as short as 50-100 km for hectometric waves. It is shown that interactions with a low frequency  $E_{\parallel}$  turbulence, for example due to inertial Alfvén waves, located above the ionosphere may explain their generation. This possible role of Alfvén waves in the acceleration was already explored by *Hess et al*, [2007], and *Mottez et al*, [2010] in the context of the Io-related S-bursts.

A first comment concerns the strong efficiency of the conics for the CMI. The largest CMI growths are obtained with ideal ring distribution,  $(1/2\pi v_0)\delta(v_{\perp}-v_0)\delta(v_{\parallel})$  [*Pritchett*, 1986, *Le Quéau and Louarn*, 1989], leading to  $\gamma/\omega_c \sim 1/2 (v_0/c)^2$ , meaning  $10^{-2}$  for 5 keV electrons. Our estimated growths are 2-3 smaller, still 5-10 larger than those estimated from the loss cone *Louarn et al* [2017]:  $\gamma/\omega_c \sim 4 \times 10^{-3}$  as compared to  $5 \times 10^{-4}$  with the loss cone. To some extent, the conics optimize the positive  $\partial f / \partial v_{\perp}$ : electrons concentrate in the conic angular sector which leads to local phase space density an order of magnitude larger than at other pitch angles. Indeed, the conic phase space densities are typically 5 times larger than measured with the loss cone distribution studied in *Louarn et al*, [2017], at similar velocities and for comparable densities ( $\sim 10 \text{ cm}^{-3}$ ).

The second comment is about the relationship with the acceleration process. At Earth, the discovery of a close link between the auroral particle acceleration and the generation of the AKR – i.e. that the source or radiation are also regions where a finite  $E_{\parallel}$  develops- was a significant advance in space physics. With FAST observations, it was also possible to establish that Alfvénic acceleration may occasionally trigger the generation of radio emission at Earth [Sue *et al*, 2007]. The present study suggests that this is more the rule than the exception at Jupiter, with a different scenario: the radio generation is linked to conics that are possibly generated by low frequency turbulence able to contribute to the electron precipitation and the formation of auroral forms. This form of efficient free energy is widely spread along the field lines and, since the condition  $(f_p/f_c)^2 \ll 1$  is easily fulfilled at Jupiter, the CMI can develop in a large altitude range. The sources are then not restricted to the plasma cavity formed by the accelerated electric field.

### **Acknowledgments and Data**

The French part of this works is supported by CNRS and CNES. The research at the University of Iowa was supported by NASA through contract 699041X with Southwest Research Institute. The JNO-E/J/SS-WAV-3-CDR-SRVFULL-V1.0, JNO-J/SW-JAD-3-CALIBRATED-V1.0 and JNO-J/SW-JAD-2-UNCALIBRATED-V1.0 data sets were obtained from the Planetary Data System (PDS) at <http://pds.nasa.gov/>.

### **References**

André, M. and Eliasson, L. (1992): Electron acceleration by low frequency electric field fluctuations – Electron conics, *Geophys. Res. Lett.*, 19, 1073–1076,  
doi:10.1029/92GL01022

Bagenal, F. et al. (2017), Magnetospheric science objectives of the Juno mission, *Space Sci. Rev.*, 213, 219-287, doi:10.1007/s11214-014-0036-8.

Chaston, C., J. Bonnell, C. Carlson, M. Berthomier, L. Peticolas, I. Roth, J. McFadden, R. Ergun, and R. Strangeway (2002), Electron acceleration in the ionospheric Alfvén resonator, *J. Geophys. Res.*, 107(A11), 1413, doi:10.1029/2002JA009272.

Connerney, J. E. P., Benn, M., Bjarno, J. B., Denver, T., Espley, J., Jorgensen, J. L., Jorgensen, P. S., Lawton, P., Malinnikova, A., Merayo, J. M., Murphy, S., Odom, J., Oliverson, R., Schnurr, R., Sheppard, D., Smith, E. J. (2017) The Juno Magnetic Field Investigation, *Space Sci. Rev.*, doi: 10.1007/s11214-017-0334-z

Delory, G. T., R. E. Ergun, C. W. Carlson, L. Muschietti, C. C. Chaston, W. Peria, J. P. McFadden, and R. Strangeway (1998), FAST observations of electron distributions within AKR source regions, *Geophys Res Lett*, 25(12), 2069-2072, doi:10.1029/98gl00705.

Eliasson, L., André, M., Lundin, R., Pottellette, R., Marklund, G., and Holmgren, G. (1996): Observations of electron conics by the Viking satellite, *J. Geophys. Res.*, 101, 13225–13238, doi:10.1029/95JA02386.

Génot, V.; Louarn, P. and F. Mottez (2001), Fast evolving spatial structure of auroral parallel electric fields, *J. Geophys. Res.*, Volume 106 (12), 29633-29644, doi: 10.1029/2001JA000076

Goertz, C. K., and R. W. Boswell (1979), Magnetosphere- ionosphere coupling, *J. Geophys. Res.*, 84, 7239, doi: 10.1029/JA084iA12p07239

Hess, S., Mottez F. and P. Zarka, (2007), Jovian S-burst generation by Alfvén waves, *J. Geophys. Res.*, 112, A11212, doi: 10.1029/2006JA012191

Hultqvist, B., R. Lundin, K. Stasiewicz, L. Block, P.A. Lindqvist, G. Gustaffson, H.

Koskinen, A. Bahnsen, T.A. Potemra, and L.J. Zanetti, Simultaneous observations of upward moving field-aligned energetic electrons and ions on auroral field lines, *J. Geophys. Res.*, 93, 9765, doi: 10.1029/JA093iA09p09765

*Geophys. Res.*, 93, 9765, doi: 10.1029/JA093iA09p09765

Kletzing, C. A., Electron acceleration by kinetic Alfvén waves (1994), *J. Geophys. Res.*, 99, 11,095, doi: 10.1029/94JA00345

Kurth, W. S., G. B. Hospodarsky, D. L. Kirchner, B. T. Mokrzycki, T. F. Averkamp, W. T.

Robison, C. W. Piker, M. Sampl, and P. Zarka (2017a), The Juno Waves investigation, *Space Sci. Rev.*, doi:10.1007/s11214-017-0396-y,

Kurth, W. S., et al. (2017b), A new view of Jupiter's auroral radio spectrum, *Geophys. Res. Lett.*, 44, doi:10.1002/2017GL072889.

Le Quéau, D, R. Pellat, and A. Roux, (1984 a) Direct generation of the auroral kilometric radiation by the maser synchrotron instability - An analytical approach. *Physics of Fluids* (ISSN 0031-9171), vol. 27,247-265, doi:10.1063/1.864520.

Le Quéau, D., R. Pellat, and A. Roux (1984 b), Direct generation of the auroral kilometric radiation by the Maser synchrotron Instability: Physical mechanism and parametric study, *J. Geophys. Res.*, 89(A5), 2831–2841, doi:10.1029/JA089iA05p02831.

Le Quéau, D., and P. Louarn (1989), Analytical study of the relativistic dispersion: Application to the generation of the auroral kilometric radiation, *J. Geophys. Res.*, 94(A3), 2605–2616, doi:10.1029/JA094iA03p02605.

Louarn, P., A. Roux, H. deFéraudy, D. Le Quéau, M. André, and L. Matson (1990), Trapped electrons as a free energy source for the auroral kilometric radiation, *J. Geophys. Res.*, 95(A5), 5983–5995, doi:10.1029/JA095iA05p05983

Louarn, P., J.- E. Wahlund, T. Chust, H. de Feraudy, A. Roux, B. Holback, P. O. Dovner, A.

I. Eriksson, and G. Holmgren (1994), Observations of kinetic Alfvén waves by the Freja spacecraft, *Geophys. Res. Lett.*, 21, 1847

Louarn, P. et al (2017), Generation of the Jovian hectometric radiation: First lessons from Juno, *Geophys. Res. Lett.*, Volume 44, Issue 10, *doi:* 10.1002/2017GL072923

Louis, C. K. et al (2017), Io-Jupiter decametric arcs observed by Juno/Waves compared to ExPRES simulation, *Geophysical Research Letters*, Volume 44, Issue 18, pp. 9225-9232, *doi:* 10.1002/2017GL073036

McComas, D. J. et al. (2013) The Jovian Auroral Distributions Experiment (JADE) on the Juno Mission to Jupiter. *Space Sci Rev*, 1–97

Menietti, J. D., and J. L. Burch (1985), Electron Conic” signatures observed in the nightside auroral zone and over the polar cap, *J. Geophys. Res.*, 90(A6), 5345–5353, *doi:*10.1029/JA090iA06p05345.

Menietti, J. D.; Weimer, D. R. (1998), DE observations of electric field oscillations associated with an electron conic, *J. Geophys. Res.*, Volume 103, Issue A1, p. 431-438, *doi:* 10.1029/97JA02496

Mottez, F., Hess, S. and P. Zarka, (2010), Explanation of dominant oblique radio emission at Jupiter and comparison to the terrestrial case, *Planetary and Space Science*, 58, 1414-1422, *doi:* 10.1016/j.pss.2010.05.012

Pritchett, P. L. (1986), Cyclotron maser radiation from a source structure localized perpendicular to the ambient magnetic field, *J. Geophys. Res.*, 91(A12), 13569–13581, *doi:*10.1029/JA091iA12p13569.

Su, Y.-J., R. E. Ergun, S. T. Jones, R. J. Strangeway, C. C. Chaston, S. E. Parker, and J. L. Horwitz (2007), Generation of short-burst radiation through Alfvénic acceleration of auroral electrons, *J. Geophys. Res.*, 112, A06209, *doi:*10.1029/2006JA012131.

Thompson, B. J.; Lysak, R. L. (1996), Electron acceleration by inertial Alfvén waves,

J. Geophys. Res., Volume 101, Issue A3, p. 5359-5376, doi: 10.1029/95JA03622

Wu, C. S. and L. C. Lee, (1979) A theory of the terrestrial kilometric radiation, *Astrophys. J.*,

(230), 621-626. doi:10.1096/157120

Wu, C. S. (1985), Kinetic cyclotron and synchrotron maser instabilities - radio-emission

processes by direct amplification of radiation, *Space Sci Rev*, 41(3-4), 215-298.

Zarka, P. (1998), Auroral radio emissions at the outer planets: Observations and theories, *J*

*Geophys Res-Planet*, 103(E9), 20159-20194, doi:Doi 10.1029/98je01323.

Accepted Article

## FIGURE CAPTIONS

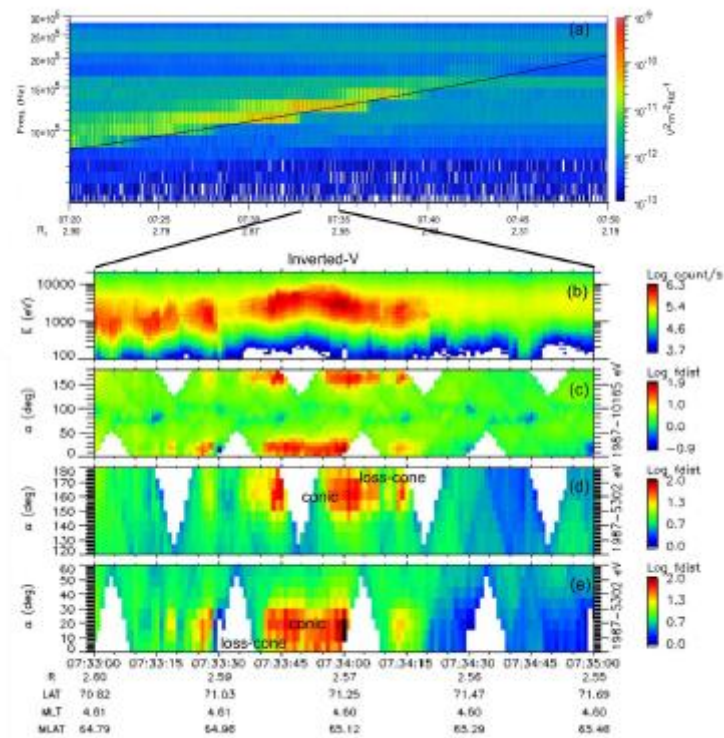


Figure 1. Combined JADE-E and Waves observations at HOM source (2017-03-27, 7:20-7:50). Panel (a): Waves dynamic spectra from 0.5 to 3 MHz. The black line is the electron gyrofrequency based on the locally measured magnetic field. Panel (b): time-energy electron flux, from 100 eV to 20 keV. Panels (c): electron pitch-angle distributions (in  $\text{km}^{-6} \text{s}^3$ ) at 2-10 keV. (white areas indicate lack of observations). Panels (d and e), zooms in the parallel and anti-parallel directions (conic angular sectors, 2-5 keV). The particle data are shown from 07:33 to 07:35, when the radio flux is maximum at  $f_c$ .

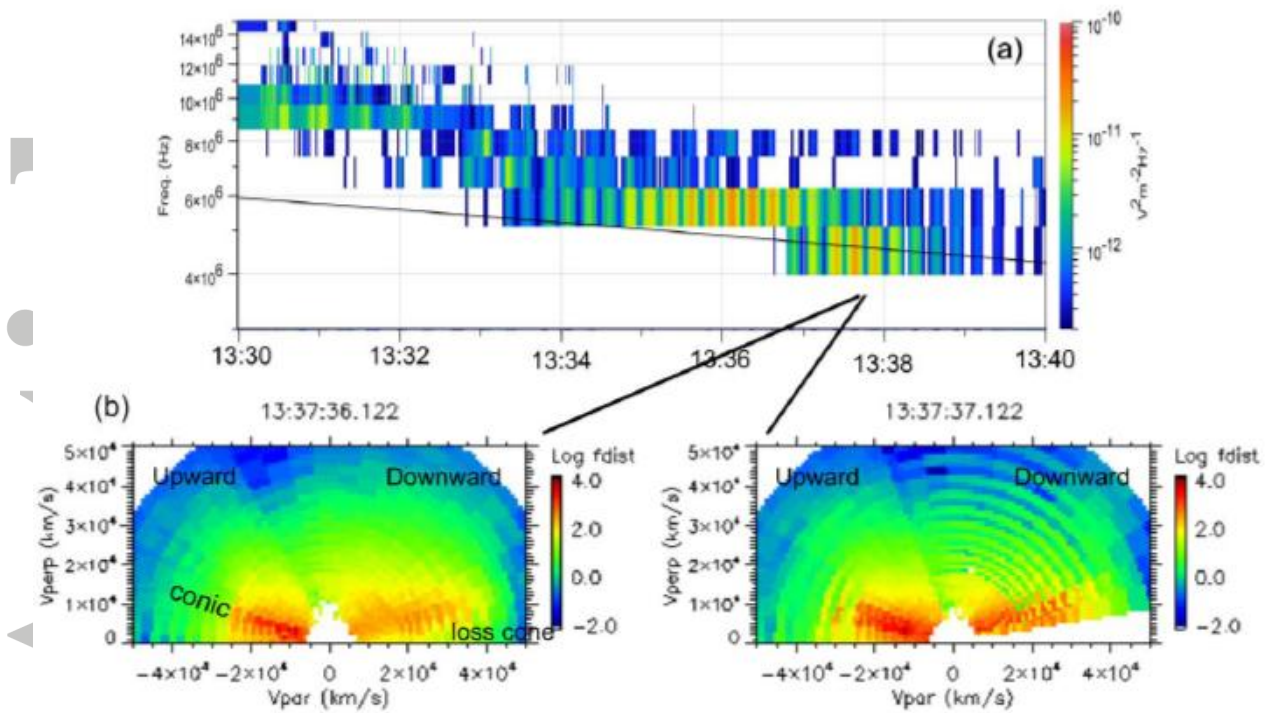


Figure 2. Second example of source crossing (2017-02-02, 13:30-13:40). Panel (a): Waves dynamic spectra from 3 to 15 MHz. Panel (b): Pitch angle distributions (in  $\text{km}^{-6} \text{s}^3$ ) measured in the source (1 s resolution). Note that this observation is made in the Southern hemisphere. By convention,  $v_{\parallel}$  is oriented in the same direction as the B-field, then positive  $v_{\parallel}$  are here directed downward, conversely to Figure 1 that presents observations made in the Northern hemisphere.

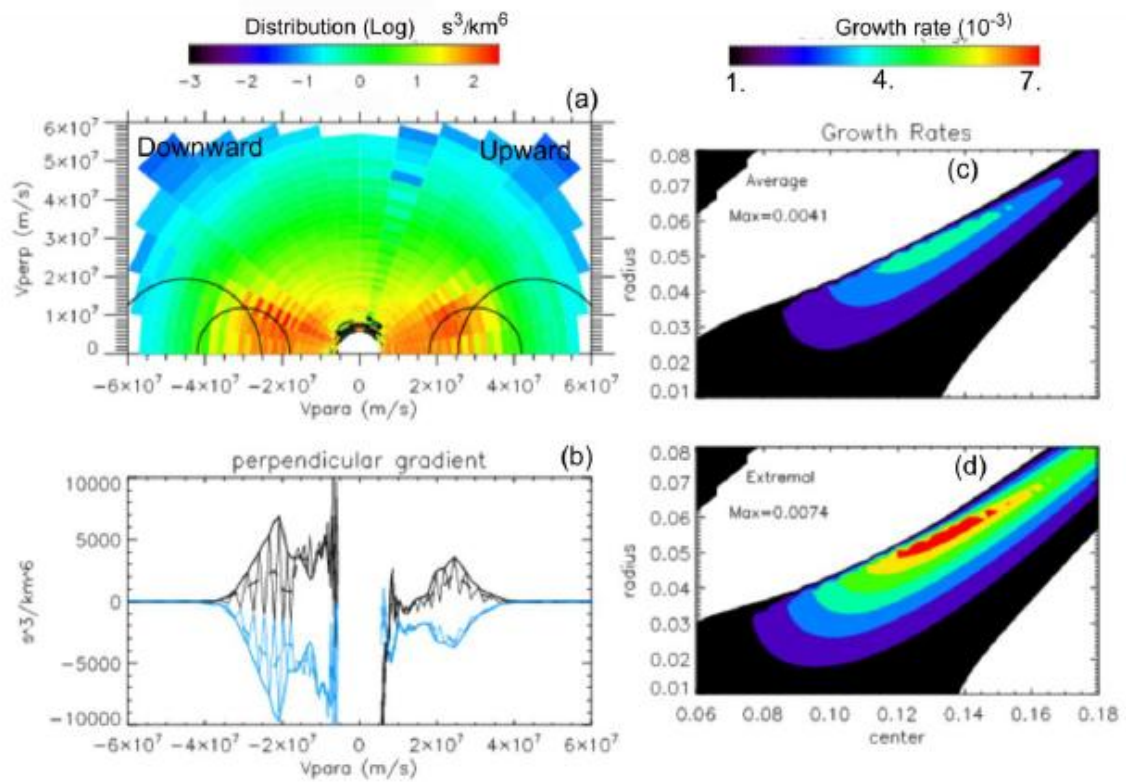


Figure 3. Panel (a): Distribution measured at 7:33:42 on day 27/03/2017 (see Figure 1). Panel (b):  $\partial f / \partial \beta_{\perp}$  gradients: in black from  $0^{\circ}$  to  $25^{\circ}$  and  $155^{\circ}$  to  $180^{\circ}$ , in blue from  $25^{\circ}$  to  $45^{\circ}$  and  $135^{\circ}$  to  $155^{\circ}$ . The extremal (average) values are indicated by continuous (dashed) lines. Panels (c, d) show contour plots of the growth rate  $\gamma/\omega_c$ , estimated from average (top) and extremal gradients (bottom).

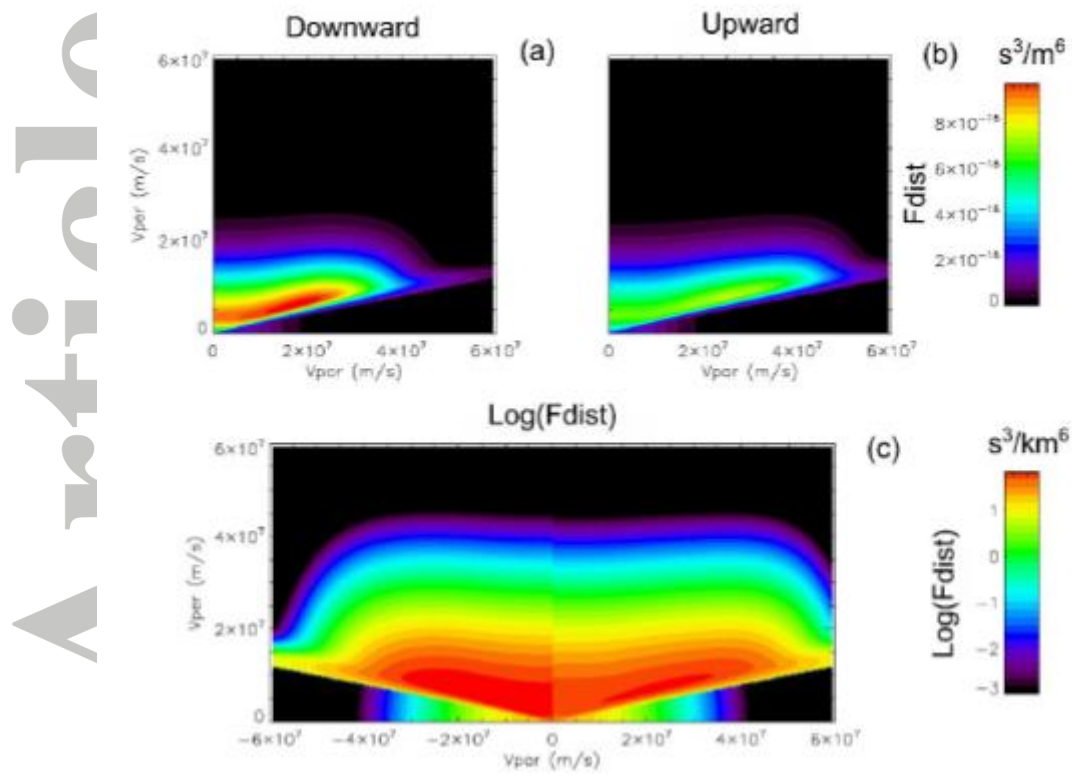


Figure 4. Simulations of conics. Top: examples obtained after interactions with the turbulence. Bottom: reconstructed conics (logarithm scale), assuming a density of  $10 \text{ cm}^{-3}$ , an initial 0.5 keV maxwellian and typical fluctuations of 10 kV above the ionosphere. The loss cone angle is  $\sim 12^\circ$ . The downward part (left side) is obtained after 1 interaction with the turbulence, the upward (right side) after 2 interactions.